Inverter Control and its Effect on Copper Losses in Electrical Machines Equipped with Hairpin Winding

Robin Krüger, Samar Singh, Patricia Penabad Durán
Mercedes-Benz AG
Stuttgart, Germany
e-mail: robin.krueger@mercedes-benz.com

Kay Hameyer, Senior Member IEEE
Institute of Electrical Machines (IEM)
RWTH Aachen University
Aachen, Germany

***Abstract*— The electric drivetrain is considered as a closed loop system consisting of the controller, the inverter and the electrical machine in this contribution. Copper losses including AC and PWM effects are studied by using two different approaches for high accuracy or fast computation, based on the finite element method (FEM) and lookup tables (LUT) respectively. The influence of switching frequency and modulation method on both inverter and copper losses is analyzed. These losses are minimized by optimizing the inverter parameters in the speed-torque map. The inverter parameter's impact on the drive cycle energy loss is discussed. A permanent magnet excited synchronous machine equipped with hairpin winding is chosen as an exemplary machine.**

Keywords*— copper losses, DPWM, hairpin winding, inverter coupling, inverter losses, PWM effects, WLTC.

I. Introduction

System efficiency is a key factor in the development of electric vehicles and can be increased by considering the interaction between different components of traction drives [1]. Therefore, the electrical machine (EM) and the inverter should be studied as one coherent electrical motor system (EMS) in an early design stage. The impact of inverter parameters on copper losses in permanent magnet synchronous machines with hairpin windings is the focus of this contribution. In addition, inverter losses are computed to analyze the losses of the EMS.

A limited amount of technical literature reports methodologies for the determination of copper losses in electrical machines considering the iteration with inverter supply. The harmonic copper losses due to inverter coupling are analytically calculated based on the harmonic spectrum of the EM currents in [1]. However, in order to apply the analytic equations, the magnetic field in the EM slots needs to be simplified. In [2], the complete electrical motor system is modelled in Simulink to study inverter effects. The EM is based on an inductance matrix obtained by flux linkages from 2D Finite Element Analysis (FEA) with sinusoidal excitation. The main disadvantage is the missing physical correlation of the actual inverter supply on the EM behavior during the FEA simulations. Directly feeding the electromagnetic FEA with determined currents is possible due to utilizing correct inductances in a lumped circuit of the inverter model [3]. An even more accurate approach for the inverter and EM coupling is a voltage driven FEA simulation [3].

In this manuscript, voltage driven transient Finite Element Analysis is used to study copper losses under pulse width modulated (PWM) voltage supply. Since this method requires high computational times, a second approach using Simulink is investigated. Here, the EMS model is built based on current lookup tables (LUT) and the analytical equations of [1] are used for copper loss calculation. In section II, the EMS, which consists of a current controller, an inverter and a permanent magnet electrical machine is introduced. Section III describes the modelling and computation of copper losses in detail. The effects of inverter switching frequency and modulation on both copper and inverter losses are analyzed in section IV. Based on the results, an optimized inverter strategy for diverse regions in the characteristic speed-torque map of the studied EMS is presented. The impact of the optimization on the sum of copper and inverter losses over the Worldwide Light Vehicles Test Cycle (WLTC) is subject of section V.

II. Electrical Motor System

A schematic view of the EMS is depicted in Figure 1. For stationary considerations, a current controller as well as an inverter model are necessary to create PWM patterns which can be used for simulating the EM. The three components which form the EMS are described in the following.

A. Current Controller

The control strategy Maximum Torque per Ampere is utilized to select the command currents $i_{\mathrm{d,cmd}}$ and $i_{\mathrm{q,cmd}}$. The current angle is increased until the terminal voltage does not exceed the maximum supply voltage of the inverter in the field weakening region. The control unit consists of two PI controllers and a Clarke- and Park transformation which regulate the EM currents i_{u}, i_{v} and i_{w} by computing the three phase modulation signals $v_{\mathrm{u,mod}}$, $v_{\mathrm{v,mod}}$ and $v_{\mathrm{w,mod}}$ for the inverter block. Therefore, Space Vector Pulse Width Modulation (SVM) is utilized as modulation strategy. It is implemented via an offset added to each of the three-phase reference voltages of the control unit [4]. The modulation voltage signals are then compared with a triangular reference

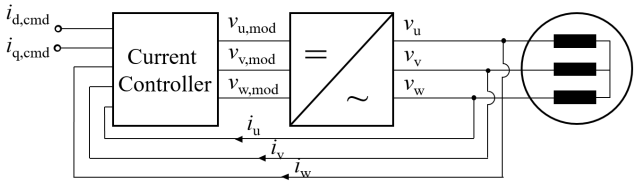

Figure 1. Schematic view of the electrical motor system.

978-1-6654-5404-9/22/$31.00 ©2022 IEEE

2022 12th International Electric Drives Production Conference (EDPC) | 978-1-6654-5404-9/22/$31.00 ©2022 IEEE | DOI: 10.1109/EDPC56367.2022.10019753

of a 10 kHz switching frequency in order to create the pulse width modulation patterns [5]. A voltage limiter is also part of the control unit to ensure the modulation signals do not exceed the maximum possible voltage of the inverter.

B. Inverter Model

Silicon Carbide (SiC) MOSFETs can fulfill the demands for highly efficient power electronics in the automotive sector [6]. Therefore, an 800 V two-level voltage source inverter (2L VSI) equipped with eight SiC MOSFETs is studied in this contribution. The inverter block creates the PWM sequence voltage assuming an ideal switching behavior of the semiconductors. Switching and conduction losses contribute to the total losses of the inverter. It is necessary to determine the time dependent currents through the individual SiC MOSFETs i_m and freewheeling diodes i_d for the calculation of inverter losses. The switching losses

$$P_\mathrm{sw} = \frac{1}{T_\mathrm{el}} \sum_0^t E_\mathrm{sw}\, s(t) \tag{1}$$

are calculated for one electrical period T_el by the switching energies E_sw at the turn-on and turn-off events which are indicated by the time dependent function $s(t)$ obtained by the simulations. The switching energy

$$E_\mathrm{sw} = E_\mathrm{on,m}(i_\mathrm{m}, u) + E_\mathrm{off,m}(i_\mathrm{m}, u) + E_\mathrm{d}(i_\mathrm{d}, u) \tag{2}$$

is the sum of turn-on and turn-off energies for the SiC MOSFETs $E_\mathrm{on,m}$, $E_\mathrm{off,m}$ and the diodes E_d. All depend on the actual current and voltage at the individual components. The conduction losses

$$P_\mathrm{cond} = \frac{1}{T_\mathrm{el}} \int_0^t p_\mathrm{cond}(t)\, dt \tag{3}$$

can be determined over one electrical period with

$$p_\mathrm{cond} = i_\mathrm{m}^2(t)\, r_\mathrm{m,ds,on}(i_\mathrm{m}) + i_\mathrm{d}(t)\, v_\mathrm{d,sd}(i_\mathrm{d}) \tag{4}$$

through the time dependent currents in the SiC MOSFETs and the diodes with their resistance $r_\mathrm{m,ds,on}$ and voltages $v_\mathrm{d,sd}$. The inverter losses are part of the system losses besides the losses in the electrical machine.

C. Electrical Machine

The EM is an eight-pole permanent magnet excited electrical motor shown in Figure 2. The machine is equipped with hairpin windings, which enable improved copper fill ratios and cost-effective series production [7]. However, alternating current (AC) losses have to be considered due to large cross sectional areas of the hairpin windings. Their impact on drive cycle losses on an exemplary traction machine for the automotive sector is presented in [8]. The EM's maximum speed is 12,000 rpm and its peak power is 250 kW. A similar variation of the design is described in detail in [9]. The machine is used in a traction drive system and is analyzed on the characteristic speed-torque map region containing the WLTC operating points of a typical compact SUV vehicle. Two different methods for the 2D simulation of the EMS are investigated in this section. The first approach uses voltage driven FEA simulations for high accuracy. The second approach is based on a LUT built Simulink model and utilizes analytical equations for computing the copper losses. Both methods require an initial simulation for the calculation of magnetic flux and inductances.

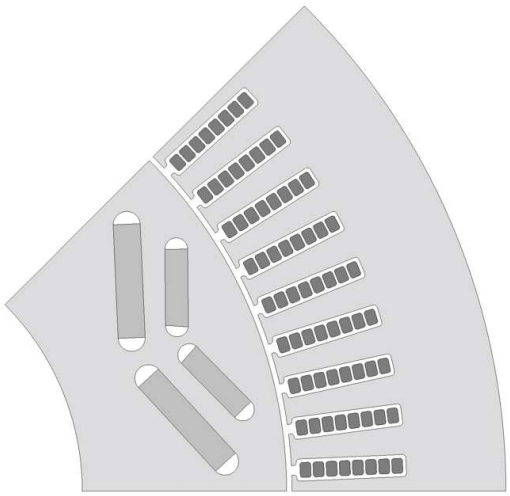

Figure 2. Electrical machine design similar to [9].

III. Simulations

A. FEA Method

In the FEA Method the entire EMS is built in the electromagnetic simulation software JMAG [10]. The voltage driven transient FEA is used to study copper and inverter losses over the characteristic speed-torque map. The transient signals for the three phase currents and switching states are used to calculate the inverter losses based on the equations in the previous section. The current density distribution needs to be known for copper loss computation including AC and PWM effects. Hence, Maxwell's equations for time-varying electromagnetic fields have to be employed [11] to compute the current density in the winding. With the knowledge of the FEA current density distribution $\boldsymbol{J}_i$, the overall copper losses can be obtained via

$$P_\mathrm{Cu,FEA} = \sum_{i=1}^{n} \boldsymbol{J}_\mathrm{i}^2 / \sigma_\mathrm{i} v_\mathrm{i} \tag{5}$$

with the copper conductivity σ_i and v_i the volume of the finite element *i*. The temperature of 80°C is considered in the stator windings for all copper loss calculations and current displacement effects in the end windings are neglected.

B. LUT Method

The second method models the entire EMS in Simulink. The EM is implemented by the differential equations for the magnetic flux in d-axis

$$\dot{\Psi}_\mathrm{d} = v_\mathrm{d} + \omega\, \Psi_\mathrm{q} - R_\mathrm{ph} i_\mathrm{d} \tag{6}$$

and q-axis

$$\dot{\Psi}_\mathrm{q} = v_\mathrm{q} - \omega\, \Psi_\mathrm{d} - R_\mathrm{ph} i_\mathrm{q} \tag{7}$$

using voltages v_d, v_q coming from the inverter, angular frequency ω, phase resistance R_ph and lookup tables for $i_\mathrm{d}(\Psi_\mathrm{d}, \Psi_\mathrm{q}, \vartheta_\mathrm{el})$ and $i_\mathrm{q}(\Psi_\mathrm{d}, \Psi_\mathrm{q}, \vartheta_\mathrm{el})$ based on initial FEA simulations with sinusoidal excitation. The three phase currents i_u, i_v and i_w are obtained by Inverse Clarke- and Park transformation and a Fast Fourier Transform (FFT) is performed. The current spectrum can be utilized to compute copper losses including AC and PWM effects analytically by the following equations. The increase factor for copper losses

$$k_{\mathrm{ru}} = \frac{R_{\mathrm{ac}}}{R_{\mathrm{dc}}} \tag{8}$$

is defined by the resistance R_{ac} including current displacement effects and the dc resistance R_{dc}. It can be calculated by

$$k_{\mathrm{ru}} = b_{\mathrm{c}}^2 / I^2 \int_0^{h_{\mathrm{c}}} \boldsymbol{J}\boldsymbol{J}^* \, dy \tag{9}$$

with the conductor's height h_{c} and width b_{c} as well as current density J and current I [12]. A practical solution for equation (9) is given in [13] assuming a purely transverse B-field in the slot. The increase factor for rectangular shaped conductors which are commonly used in hairpin windings can be calculated by

$$k_{\mathrm{ru}} = \varphi(\beta) + p(p-1)\,\Psi(\beta) \tag{10}$$

with p being the conductor's number and the two auxiliary functions

$$\varphi(\beta) = \beta \frac{\sinh 2\beta + \sin 2\beta}{\cosh 2\beta - \cos 2\beta} \tag{11}$$

$$\Psi(\beta) = 2\beta \frac{\sinh \beta + \sin \beta}{\cosh \beta - \cos \beta} \tag{12}$$

using

$$\beta = h_{\mathrm{c}} \sqrt{\pi f \, \mu_0 \, \sigma_{\mathrm{c}} \, b_{\mathrm{c}} / b_{\mathrm{slot}}} \tag{13}$$

based on geometrical parameters for sub-conductors and slot width b_{slot}, frequency f as well as permeability of free space μ_0 and electrical conductivity σ_{c}. In order to account for PWM effects the harmonic currents I_{n} for occurring orders n must be extracted from the FFT of the phase currents. The increase factor k_{ru} must be computed for the existing orders n of the electrical frequency f_{el} separately. The copper losses including AC and PWM effects can then be calculated by the sum of copper losses for the separated frequencies [1]:

$$P_{\mathrm{cu,analytic}} = \sum_{n \geq 1} k_{\mathrm{ru}}(n\, f_{\mathrm{el}})\, R_{\mathrm{dc}}\, I_n^2 \,. \tag{14}$$

C. Simulation Results

The simulation results for copper losses of both presented methods are compared in an exemplary operating point at 6000 rpm speed and low torque. The current spectrum of both methods for the considered operating point is shown and compared with measurement data in Figure 3. However, due to the measurement sampling frequency, the measurement data is only available up to the first switching base-frequency harmonic components. In general, a good match between simulations and measurement can be seen. However, the LUT Method contains additional low order harmonics in contrast to the measurements and the FEA Method. Therefore, the FEA Method with higher accuracy expectations aligns better with measurements. For the switching base-frequency and its multiples the alignment between FEA and LUT methods shows a remarkable quality. The copper losses of both EMS simulation methods for the sample operating point are shown in Table I. Copper losses of the FEA method are 10.5W higher than the corresponding losses of the LUT method. However, simulation time differs significantly. Once the initial simulation is performed and the models are set up, the FEA method requires a simulation time of approximately 1.5 hours for the analyzed operating point due to the complex FEA calculations for fine time steps. In contrast, the LUT method can be carried out within less than one minute for the same time steps after the model setup.

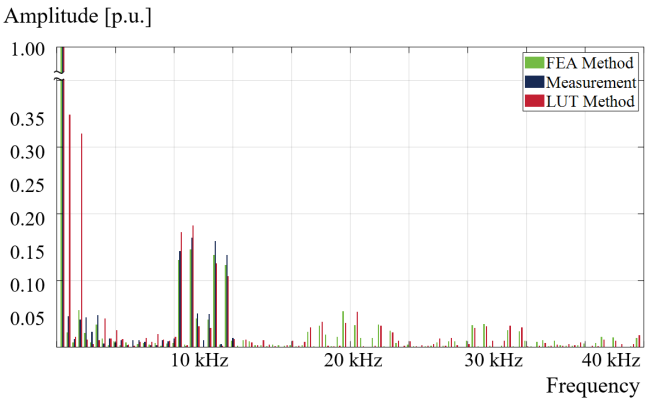

Figure 3. Harmonics of EM phase current using SVM as modulation.

EMS Simulation Method	Total Copper Losses
FEA Method	128.8 W
LUT Method	118.3 W

Table I. Comparison in copper losses for both EMS simulation methods.

High computational capacity is required to simulate a sizeable amount of operating points with the FEA approach in order to form a speed-torque map. Operating points for very low speeds are neglected due to their extremely high simulation times based on their small step size compared to the electrical period. Hence, the speed axis starts at 1/12 of the maximum speed. Fig. 4 and 5 show the normalized inverter and copper losses respectively scaled to the maximum sum of both.

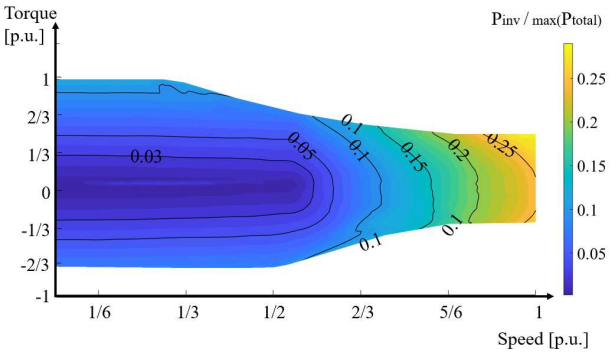

Figure 4. Inverter losses for FEA Method.

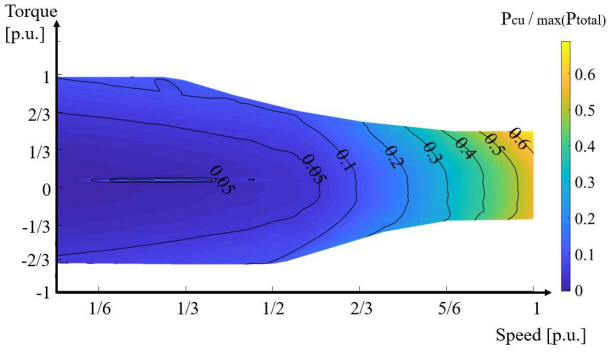

Figure 5. Copper losses for FEA Method.

The highest losses occur at the peak torque for maximum speed where the copper losses are significantly higher than the inverter losses of the analyzed EMS. In the next step, copper losses were determined drastically faster for the same operating points with the LUT method. The comparison of copper losses for both approaches is shown in Figure 6 by the division of copper losses of the LUT method by the copper

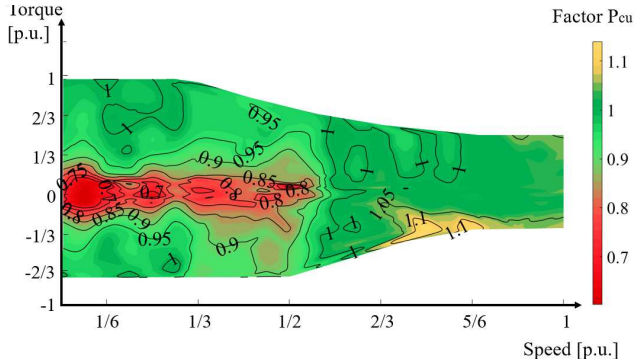

Figure 6. Copper Loss Factor: LUT / FEA Results.

losses of the FEA method. There exists a reasonable deviation of ±5% in the widest range of the speed-torque map. However, higher differences can be seen for lower torque values in the constant torque region. The discrepancy for this particular region can be traced back to the assumptions for analytically calculating the AC copper losses. The assumption of a purely transverse B-field in the slot is inadequate for low torque values in the constant torque region [9]. Not only the influence of permanent magnets but also reluctance paths in the rotor and material effects create longitudinal components in the B-field of the stator slots. These components are neglected in the determination of the factor k_{ru} using (10). Consequently, the copper losses of the LUT simulation method are lower than the copper losses of the FEA method in this region. Hence, the FEA method is utilized for further investigations due to the physical limitation of the LUT approach, better matching FFT currents with the measurement data and higher accuracy expectations.

IV. Inverter Parameter Optimization

The benefit of taking the inverter supply into account for EM simulations is to investigate on different influences on system losses. Therefore, inverter parameters and their effect on both inverter losses and EM losses can be studied. In this paper, several inverter parameters are optimized with respect to minimal inverter plus copper losses. Hence, inverter P_{inv} and copper losses P_{cu} are summed to form total losses P_{total}. Iron and magnet losses are neglected in this contribution. The controller and its parameters are kept constant for all studies.

A. Modulation Strategy

The modulation strategy is one important inverter parameter which can be used to improve the electric drive system efficiency [14]. SVM as a continuous PWM method is compared to various Discontinuous Pulse Width Modulation (DPWM) types where no switching in the semiconductors occurs for a certain part of one electrical period. Thus, switching losses in the inverter can be significantly reduced. Figure 7 illustrates all studied modulation types of this contribution. All types are integrated in the EMS models by an offset added to each of the three-phase reference voltages [16]. The influence of the modulation type on copper as well as inverter losses is studied. Figure 8 shows the optimal DPWM method for lowest inverter losses of the analyzed EMS. The change in inverter losses of the optimized modulation strategy compared to the SVM reference is illustrated in Figure 9. It can be seen the inverter losses decrease by more than 15-20% for the most parts of the speed-torque map. However, DPWM methods generally increase the current harmonics and consequently copper losses in the EM.

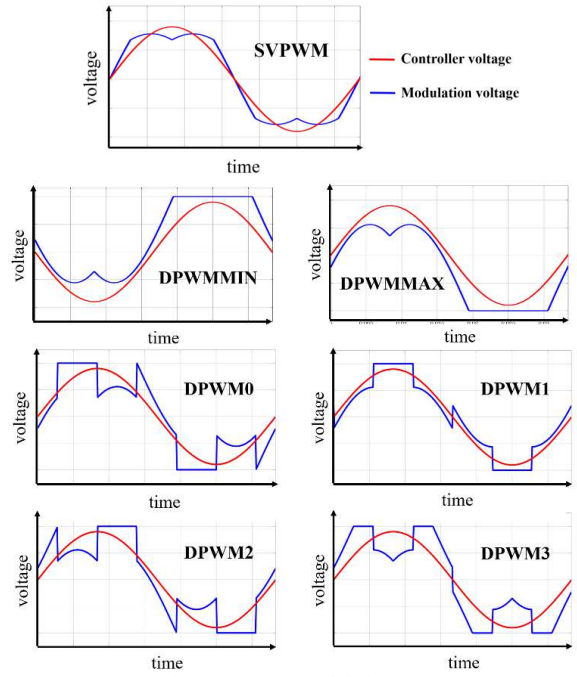

Figure 7: PWM modulation [15].

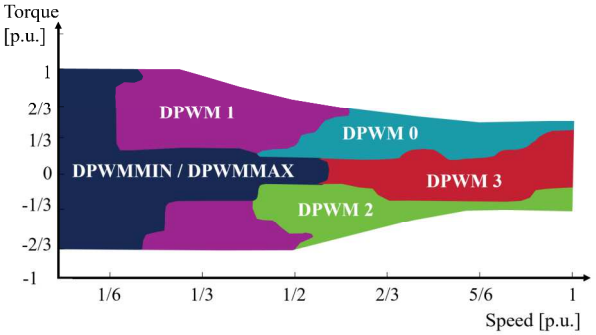

Figure 8: Optimized modulation strategy for minimal inverter losses.

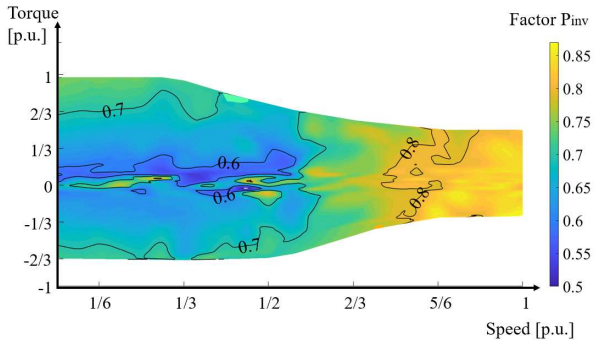

Figure 9: Inverter losses: Optimized modulation / SVM reference.

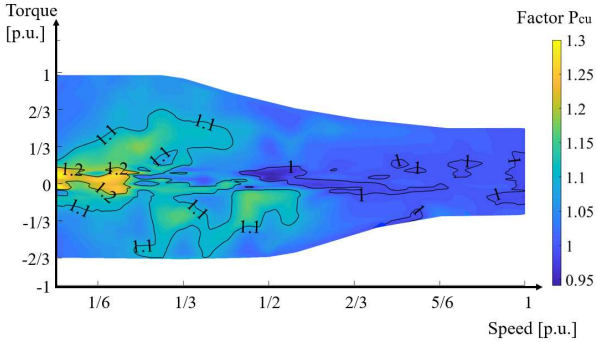

Figure 10: Copper losses: Optimized modulation / SVM reference.

The copper losses of the optimized modulation strategy are compared to the SVM reference in Figure 10.

B. Switching Frequency

Furthermore, the switching frequency has an impact on both inverter losses and losses in the electrical machine. Besides the 10 kHz switching frequency for the SVM reference EMS, the switching frequencies of 6 kHz, 8 kHz and 12 kHz are utilized. The modulation type SVM is kept constant for the comparison. At first, inverter and copper losses are compared between the switching frequencies 10 kHz and 6 kHz in Figure 11 and 12 respectively. On the one hand, the increase in switching frequency causes more inverter losses over the entire speed-torque map. On the other hand, a higher switching frequency reduces the copper losses in the EM. Therefore, a tradeoff has to be found for the optimization of the system losses. Figure 13 shows the optimal switching frequency for the total losses. The total losses can significantly be decreased for low speed but also be reduced around 5-10% in the field weakening region by optimizing the switching frequency compared to the 10 kHz reference (Figure 14).

C. Overall

The influence of inverter modulation strategy and switching frequency was analyzed in the previous paragraphs. Both inverter parameters were optimized for diverse regions in the speed-torque map separately. In a final step, the results from switching frequency and modulation strategy variation are combined to form an optimal inverter parameter strategy for the different regions in the speed-torque map. Results for the switching frequency variation of SVM and the modulation type DPWM are optimized with respect to minimal inverter plus copper losses. Figure 15 shows the optimal inverter strategy for the total losses. SVM modulation shows the minimal losses for low speed and also low torque regions in the constant torque region. The switching frequency is adapted to higher values for the region with low torque increasing with speed. Various DPWM methods are beneficial for the total losses in the field weakening region and also for higher torque operating points in the constant torque region.

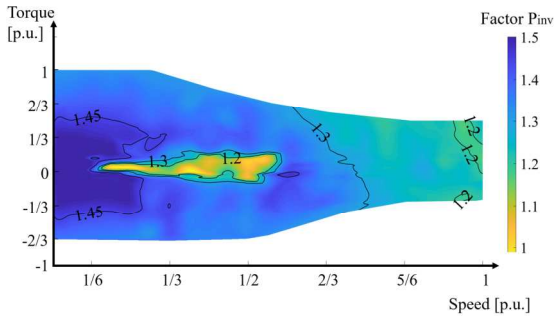

Figure 11. Inverter losses: SVM 10kHz/6kHz.

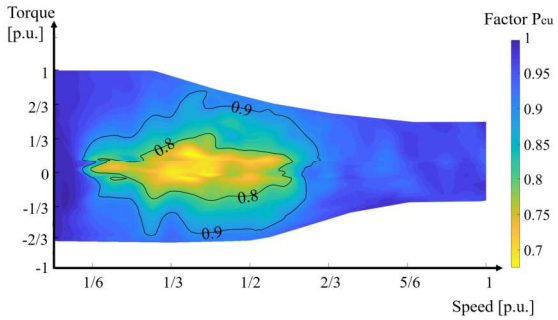

Figure 12. Copper losses: SVM 10kHz/6kHz.

There exist also deviations for certain parts of the speed-torque map when comparing Figure 15 with Figure 8 due to the different optimization goals. In contrast to the optimization for total losses in Figure 15, the optimization for inverter losses is performed in Figure 8. The benefit of the optimized inverter parameters is shown in Figure 16 with lower total losses over the entire speed-torque map.

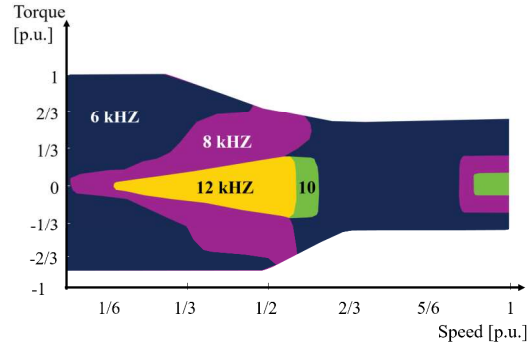

Figure 13. Optimal switching frequency for total losses.

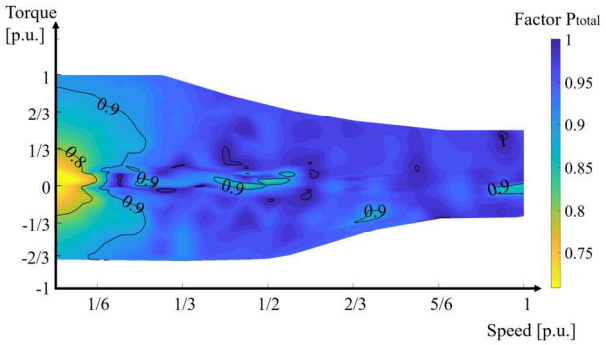

Figure 14. Total losses: Optimized switching frequency / 10kHz ref.

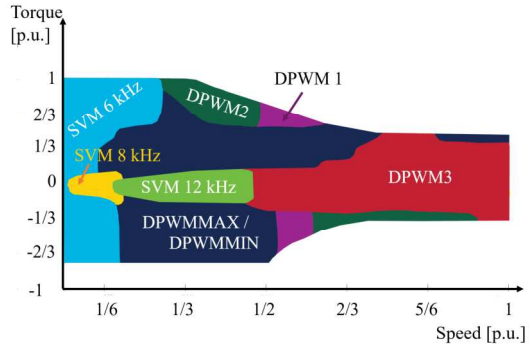

Figure 15. Optimal inverter parameter for total losses.

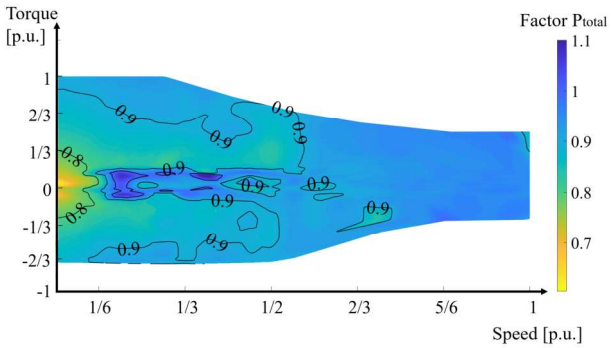

Figure 16. Total Losses: Opt. inverter parameters / 10 kHz SVM ref.

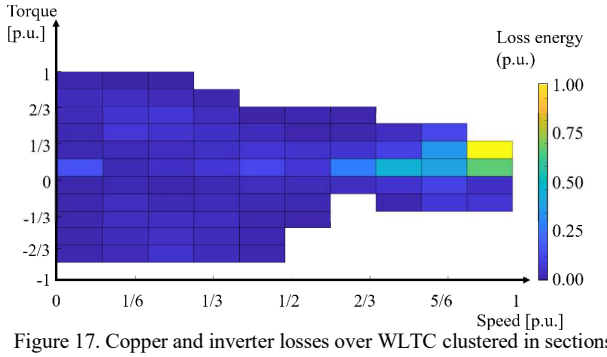

Figure 17. Copper and inverter losses over WLTC clustered in sections.

	SVM Reference	Optimized Inverter Parameters
Copper + Inverter losses	1 p.u.	0.94 p.u.

Table II. Comparison in copper and inverter loss energies over WLTC.

V. Influence on the WLTC

The impact of reduced copper and inverter losses due to optimized inverter parameters over the WLTC are analyzed for an exemplary compact SUV. The loss energy of copper and inverter losses for the optimized inverter parameter strategy over the entire cycle is clustered in 10 sections for speed and 11 for torque axis and depicted in Figure 17. The extremely time consuming simulations for low speed values are performed once with the reference inverter parameter set in order to fit in all operating points of the cycle. The outcome is attached to the operating point results for the optimized inverter parameters. However, these low speed operating points contribute to the loss energy over the WLTC marginally (see Figure 17). The highest loss energy can be found at peak torque for the highest speed. The loss energy for copper and inverter losses is determined for the reference inverter parameter set and compared to the corresponding loss energy with the optimized inverter strategy in Table II. The reduction of copper and inverter loss energy over WLTC of 6% can be reached by optimization of inverter parameters for different regions in the speed-torque map.

VI. Conclusion

The EMS is considered as one coherent system in this paper. Its different parts – control unit, inverter and electrical machine – are described in detail. Two different methods for simulating the EMS are focused with the target of determining copper losses. The FEA method uses voltage driven FEA simulations and delivers high accuracy results. The drawback is the high computational time. The second approach uses a LUT model for obtaining phase currents and uses analytical equations based on the machine geometry, materials and the current FFT. The simulation time of this approach is drastically lower by showing similar copper loss values for a wide range of the speed-torque map. However, certain areas of the speed-torque map are pointed out where the LUT method shows physical limitations. In addition, inverter losses are computed for the considered 2L VSI with SiC MOSFETs. The inverter parameters switching frequency and modulation strategy and their influence on both copper and inverter losses are studied. A higher switching frequency causes reduced copper but increased inverter losses. Various DPWM methods are analyzed and an optimum strategy for the different parts of the speed-torque map is developed for minimum inverter losses of the considered EMS. Furthermore, an optimization of inverter parameters with the target of minimizing copper plus inverter losses is found for the reference EMS. The losses can be reduced and the loss energy over the WLTC of an exemplary SUV is decreased by about 6 % by alternating the switching frequency for SVM and utilization of various DPWM methods in diverse parts of the speed-torque map. Consequently, system losses can be reduced by considering the interaction between diverse components of traction drives in an early design stage.

References

[1] T. Velic, M. Barkow, D. Bauer, P. Fuchs, J. Wende, T. Hubert, M. Reinlein, J. Nägelkrämer and Nejila Parspour, "Efficiency Optimization of Electric Drives with Full Variable Switching Frequency and Optimal Modulation Methods," 17th Conference on Electrical Machines, Drives and Power Systems (ELMA), pp. 1-6, 2021.

[2] M. van der Geest, H. Polinder and J. A. Ferreira, „Influence of PWM switching frequency on the losses in PM machines," International Conference on Electrical Machines (ICEM), pp. 1243-1247, 2014.

[3] G. Volpe, M. Popescu, L. Di Leonardo and S. Xue., "Efficient Calculation of PWM AC Losses in Hairpin Windings for Synchronous BPM Machines", IEEE International Electric Machines & Drives Conference (IEMDC), 2021.

[4] R. Maheshwari, S. Busquets-Monge and J. Nicolas-Apruzzese, "A Novel Approach to Generate Effective Carrier-Based Pulsewidth Modulation Strategies for Diode-Clamped Multilevel DC–AC Converters," in IEEE Transactions on Industrial Electronics, vol. 63, no. 11, pp. 7243-7252, 2016.

[5] H. Abu-Rub, A. Iqbal, J. Guzinski, "High Performance Control of AC Drives with MATLAB/Simulink Models," (2nd edn.), John Wiley and Sons Ltd., p. 49-66, 2021.

[6] M. Kilper, S. Fickel, H. Naumoski and K. Hameyer, "Effects of Fast Switching Semiconductors Operating Variable Speed Low Voltage Machines," 2019 9th International Electric Drives Production Conference (EDPC), 2019, pp. 1-7, doi: 10.1109/EDPC48408.2019.9011884.

[7] T. Glaessel, D. B. Pinhal, M. Masuch, D. Gerling and J. Franke, "Manufacturing Influences on the Motor Performance of Traction Drives with Hairpin Winding," 2019 9th International Electric Drives Production Conference (EDPC), 2019, pp. 1-8, doi: 10.1109/EDPC48408.2019.9011872.

[8] D. B. Pinhal and D. Gerling, "Driving Cycle Simulation of Wound-Rotor Synchronous Machine with Hairpin Windings Considering AC-Losses," 2019 IEEE Transportation Electrification Conference and Expo (ITEC), 2019, pp. 1-7, doi: 10.1109/ITEC.2019.8790556.

[9] R. Krüger, P. Penabad Durán and K. Hameyer, "Research on ac copper losses in permanent magnet electrical machines with hairpin windings for automotive applications", Eur. Phys. J. Appl. Phys. 97 34 (2022),

[10] JMAG-Designer FEA Software Tool (Ver. 21.0). [online]. Available: https://www.jmag-international.com/products/jmag-designer/, (accessed October 25, 2022)

[11] K. Hameyer and R. Belmans, "Numerical Modelling and Design of Electrical Machines and Devices," WIT Press, Southampton, United Kingdom, 1999.

[12] J. Pyrhonen, T. Jokinen, V. Hrabovcova, Design of rotating electrical machines, 2nd edn. (Wiley, Chichester, United Kingdom, 2008)

[13] G. Müller, K. Vogt, B. Ponick, Berechnung elektrischer Maschinen, 6th edn. (Wiley-VCH, Weinheim, Germany, 2008).

[14] G. Zu, X. Zhu and S. Yang, „Using DPWM method to improve system efficiency of the macine drive system", 22nd International Conference on Electrical Machines and Systems (ICEMS), (2019).

[15] A. Hava, R. Kerkman, T. Lipo, "A High-Performance Generalized Discontinuous PWM Algorithm", IEEE Transactions on Industry Applications vol. 34, no. 5, (1998).

[16] O. Ojo, "The generalized discontinuous PWM scheme for three-phase voltage source inverters," in IEEE Transactions on Industrial Electronics, vol. 51, no. 6, pp. 1280-1289, Dec. 2004, doi: 10.1109/TIE.2004.83791.